FLC-Based DTC Scheme to Improve the Dynamic Performance of an IM Drive

M. Nasir Uddin, *Senior Member, IEEE*, and Muhammad Hafeez

***Abstract*—This paper presents a fuzzy logic hysteresis comparator-based direct torque control (DTC) scheme of an induction motor (IM) under varying dynamic conditions. The fuzzy logic controller (FLC) is used to adjust the bandwidth of the torque hysteresis controller in order to reduce the torque and flux ripples and, hence, to improve motor dynamic response. The effects of torque hysteresis bandwidth on the amplitude of torque ripples of an IM are also discussed in this paper. Based on the slopes of motor-estimated torque and stator current, an FLC is designed to select the optimum bandwidth of the torque hysteresis controller. This paper also proposes a simpler algorithm than the conventional trigonometric function-based algorithm to evaluate the sector number (required for DTC scheme) of the stator flux-linkage space vector. The proposed algorithm reduces the computational burden on the microprocessor. In order to test the performance of the proposed FLC-based DTC scheme for IM drive, a complete simulation model is developed using MATLAB/Simulink. The proposed FLC-based DTC scheme is also implemented in real time using DSP board DS1104 for a prototype 1/3 hp motor. The performance of the proposed drive is tested in both simulation and experiment.**

***Index Terms*—Direct torque control (DTC), field-oriented control (FOC), fuzzy logic controller (FLC), induction motor (IM), torque and flux hysteresis controllers, torque ripples.**

I. Introduction

THE advantages of direct torque control (DTC) over its competitor field-oriented control (FOC) are well known [1]. The DTC utilizes hysteresis band controllers for both stator flux-linkage and motor-developed torque controls. Unlike FOC, the DTC scheme does not need any coordinate transformation, pulsewidth modulation (PWM), and current regulators. The PWM stage takes almost ten times longer processing time than the DTC to respond to the actual change [2]. The DTC uses flux and torque as primary control variables which are directly obtained from the motor itself. Therefore, there is no need for a separate voltage and frequency controllable PWM. This characteristic makes the DTC simpler and much faster in responding to load changes as compared to the FOC. The major problem in a DTC-based motor drive is the presence of ripples in the motor-developed torque and stator flux. Generally, there are two main techniques to reduce the torque ripples. The first one is to use a multilevel inverter [3] which will provide the more precise control of motor torque and flux. However, the cost and complexity of the controller increase proportionally. The other method is space vector modulation [4]. Its drawback is that the switching frequency still changes continuously.

Advantages of intelligent controllers such as fuzzy logic, neural network, neuro-fuzzy, etc., are well known as their designs do not depend on accurate mathematical model of the system and they can handle nonlinearity of arbitrary complexity [5]–[7]. Among different intelligent algorithms, fuzzy logic is the simplest, and it does not require intensive mathematical analysis [5], [7]. Artificial intelligence-based controllers have been used by the researchers for the minimization of torque and stator flux ripples in DTC scheme-based induction motor (IM) drives [6], [8]–[13]. In [6], the authors have used a proportional-integral (PI) and fuzzy logic controller (FLC)-based hybrid speed controller. It uses an FLC in the transient state and a PI controller in the steady state. The switching mechanism between the two controllers is based on the speed error between the reference and actual speed of the motor. The threshold of the switching limit for the two controllers is based on the sampling frequency and the type of FLC used. This feature makes the switching transition complicated. Moreover, the PI controller is used in the steady state which, inherently, is motor parameter and disturbance dependent. The FLC used by every author of [8]–[10] has two input variables. Each variable has seven membership functions, and the controller uses 49 fuzzy rules to evaluate the output. Due to high computational burden of the controller, each work is not embodied by the real-time implementation and is only supported by the simulation results. The authors [11]–[13] have replaced the classical DTC switching table by an artificial intelligence-based switching mechanism to produce the inverter input voltage vector. The implementation of these schemes is almost impossible in real time due to high computational burden of the selected neural and fuzzy network. In particular, the author of [11] has used three input variables with 3, 5, and 12 membership functions. The controller uses 240 rules to evaluate the output. Another strategy to cope with the torque and ripple problem is the online updating of the torque and flux hysteresis comparator amplitude to evaluate the switching frequency of the inverter [14]. The proposed switching frequency regulator needs an output pulse counter for each hysteresis comparator. The alternate to the hysteresis comparator pulse counter is an amplitude predictor. This predictor

Manuscript received December 7, 2010; revised April 4, 2011 and September 15, 2011; accepted October 3, 2011. Date of publication December 22, 2011; date of current version March 21, 2012. Paper 2010-IACC-413.R2, presented at the 2010 Industry Applications Society Annual Meeting, Houston, TX, October 3–7, and approved for publication in the IEEE Transactions on Industry Applications by the Industrial Automation and Control Committee of the IEEE Industry Applications Society.

M. Nasir Uddin is with the Department of Electrical Engineering, Lakehead University, Thunder Bay, ON P7B 5E1, Canada (e-mail: muddin@lakeheadu.ca).

M. Hafeez is with the Thunder Bay Regional Research Centre, Thunder Bay, ON P7B 6V4, Canada (e-mail: mhafeez@lakeheadu.ca).

Color versions of one or more of the figures in this paper are available online at http://ieeexplore.ieee.org.

Digital Object Identifier 10.1109/TIA.2011.2181287

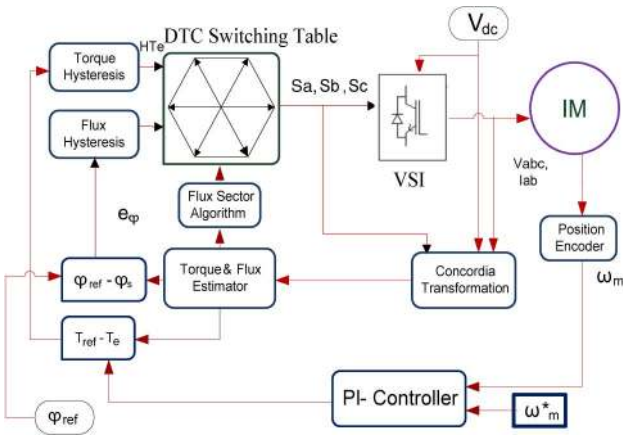

Fig. 1. Conventional DTC scheme for IM drive.

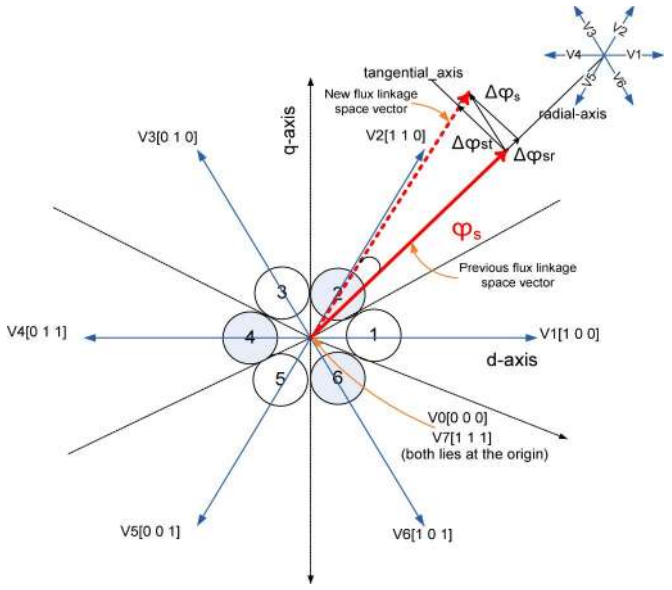

Fig. 2. VSI voltage vectors and six sectors of stator flux-linkage space vector.

is highly motor parameter and speed dependent. There is no exact strategy or formula to get the command inverter frequency. Hence, there is no real-time implementation of the work.

Some researchers have tried to minimize the ripples, keeping the constant switching frequency by evaluating the switching instant of the voltage vector to inverter [15], [16]. The authors have derived a mathematical model for motor torque slope and torque rms values. The relations are based on many assumptions and are highly motor parameter dependent. The designed model is not robust to motor parameters and load disturbances. The paper [15] does not have any real-time results. Reference [16] has some real-time results, but the implementation was not fully successful as they only provide the results at low-speed condition. Moreover, there is no real-time result under varying speed or torque commands.

Therefore, in this paper, a simpler practically feasible FLC is designed that selects the appropriate bandwidth for the torque hysteresis controller to optimize the ripple level in the developed torque and, hence, to improve the motor speed response.

Conventionally, the determination of the sector number of the stator flux-linkage space vector for the DTC scheme involves a trigonometric function (tangent) [17]. The microprocessor evaluates the trigonometric function by using time-consuming complex calculations as compared to normal arithmetic relations [18]. The requirement for the working of the DTC scheme is only the sector number, in which the stator flux-linkage space vector is positioned and not its accurate position. Therefore, this paper presents a simpler efficient algorithm to determine the stator flux-linkage sector without using any trigonometric or complex function. Hence, the proposed algorithm reduces the calculation burden for the processor.

A complete simulation model for the proposed drive is developed using MATLAB/Simulink. The proposed FLC-based DTC scheme is implemented in real time using DSP board DS1104 for a prototype 1/3 hp motor. The effectiveness of the proposed drive is verified at different dynamic operating conditions by both simulation and experimental results.

II. Modeling of IM for DTC

A. Stator Voltage and Flux

The block diagram for the conventional DTC scheme of an IM drive is shown in Fig. 1 [1], [19]. Based on the three inputs (output digit of torque hysteresis controller, output digit of flux-linkage hysteresis controller, and sector number where stator flux-linkage space vector is positioned), the DTC switching table produces the logic signals S_a, S_b, and S_c. These logic signals are used to trigger the switches of the three-phase voltage source inverter (VSI) [19]. The possible six active combinations of these logic signals and the corresponding active input voltage vectors of the inverter (V_1 to V_6) are shown in Fig. 2. The three-phase output voltage of VSI, which is the input to the stator of IM, is given by [20]

$$V_{sa} = (V_{\rm dc}/3)(2S_a - S_b - S_c) \tag{1a}$$

$$V_{sb} = (V_{\rm dc}/3)(2S_b - S_c - S_a) \tag{1b}$$

$$V_{sc} = (V_{\rm dc}/3)(2S_c - S_a - S_b) \tag{1c}$$

where $V_{\rm dc}$ stands for dc link inverter voltage. The real $(V_{s\alpha})$ and imaginary $(V_{s\beta})$ components of the stator voltage vector are obtained by using the Concordia transformation as [20]

$$\begin{bmatrix} V_{s\alpha} \\ V_{s\beta} \end{bmatrix} = \begin{bmatrix} 1 & -1/2 & -1/2 \\ 0 & \sqrt{3}/2 & -\sqrt{3}/2 \end{bmatrix} \begin{bmatrix} V_{sa} \\ V_{sb} \\ V_{sc} \end{bmatrix}. \tag{2}$$

Generally, the stator flux linkage can be obtained from the stator voltage vector as [17]

$$\phi_s = \frac{1}{T_N} \int_0^t (V_s - R_s I_s) dt + \phi_{s0}. \tag{3}$$

Neglecting stator resistance R_s, it may be simplified as

$$\Delta\phi_s = V_s \Delta t. \tag{4}$$

$\Delta\phi_s$ presents the change in stator flux caused by the application of an inverter voltage vector V_s. ϕ_{so} is the stator flux linkage

at $t = 0$. The electromagnetic developed torque in IM is given by [19]

$$T_e = P\frac{L_m}{\sigma L_s L_r}|\phi_s|^*|\phi_r|^* \sin\theta_{\rm sr} \tag{5}$$

where $\sigma = 1 - (L_m^2/L_s L_r)$ is the leakage factor, P is the number of pole pairs, L_s and L_r are the stator and the rotor self-inductances, respectively, and $\theta_{\rm sr}$ is the angle between the stator (ϕ_s) and rotor (ϕ_r) flux-linkage space vectors. In the steady state, $|\phi_r|$ and $|\phi_s|$ are almost constant, and T_e depends on the torque angle $\theta_{\rm sr}$.

Fig. 2 shows the change in stator flux linkage $\Delta\phi_s$ which is caused by the application of new stator voltage vector V_3. The stator flux-linkage space vector "ϕ_s" before and after the application of vector V_3 is shown by continuous and dotted vectors, respectively. From (4), it is clear that the change in stator flux $\Delta\phi_s$ has the same direction of the applied voltage and its amplitude is dependent on the stator input voltage vector and the duration "Δt" for which this vector is applied. Fig. 2 also shows the radial component $(\Delta\phi_{sr})$ and tangential component (Δ_{st}) of $\Delta\phi_s$. The radial component $\Delta\phi_{sr}$, being in phase with ϕ_s, causes a direct change in the amplitude of the stator flux-linkage space vector. The tangential component $\Delta\phi_{st}$, being orthogonal to ϕ_s, only changes the position of stator flux-linkage space vector ϕ_s. Thus, $\Delta\phi_{st}$ indirectly controls the angle between the stator and rotor flux-linkage space vectors, i.e., the torque angle θsr, and hence, it controls the motor-developed torque (5). Therefore, $\Delta\phi_{st}$ is the torque-producing component of $\Delta\phi_s$. From Fig. 2, it can also be observed that, with respect to the current sector number of the stator flux-linkage space vector, the application of a voltage vector from the forward direction/(direction of rotation)/(anticlockwise direction) by one or two sectors increases the torque-producing component of $\Delta\phi_s$ and vice versa which is the case for the rotation in reverse direction. Similarly, the amplitude of the stator flux-linkage space vector increases by the application of a voltage vector from a sector which is one step forward/backward direction with respect to its current sector number. For example, if, currently, the stator flux-linkage space vector is lying in sector 2 and it is required to increase both the motor-developed torque and stator flux linkage, then the inverter voltage vector V_3 should be selected in the next sampling period. However, if it is required to decrease the torque but increase the flux, then the inverter voltage vector V_1 should be selected in the next sampling period. Following this pattern, one can explain the logic behind the selection of voltage vectors in the DTC switching table.

When a zero stator voltage vector (V_0, V_7) is applied, ϕ_s stops while ϕ_r continues to move forward, reducing $\theta_{\rm sr}$ as well as T_e. If the application of zero vectors is sufficiently long enough so that ϕ_r overtakes the ϕ_s vector, then $\theta_{\rm sr}$ becomes negative. It will produce the retarding torque. Hence, the duration of application of any stator voltage vector plays an important role on the torque ripple. By cyclic switching of active and zero stator voltage vectors, we can control the motor torque with optimal level of the ripple. At low rotor speeds, the ϕ_r motion is too slow to achieve rapid torque reduction. In such situation, instead of zero vectors, an active vector moving backward is the preferred choice for effective torque control. This section elaborates the idea of voltage vector selection in the DTC switching table.

B. Flux and Torque Hysteresis Controllers

For the DTC scheme, the motor-developed torque and stator flux linkage are estimated as [17]

$$T_e = \frac{3}{2}P[\phi_{s\alpha}I_{s\beta} - \phi_{s\beta}I_{s\alpha}] \tag{6}$$

$$\phi_s = \sqrt{\left(\phi_{s\alpha}^2 + \phi_{s\beta}^2\right)} \tag{7}$$

where $I_{s\alpha}$ and $I_{s\beta}$ are the direct and quadrature components of stator current, respectively. As shown in Fig. 1, these estimated values of torque and flux are compared with the corresponding command/reference values, and the error signals are delivered to the respective hysteresis controllers. On the basis of the magnitude of the error signals and allowable bandwidth, each hysteresis controller produces a digit. Then, the position of the stator flux-linkage space vector is evaluated as

$$\theta_s = \tan^{-1}(\phi_{s\beta}/\phi_{s\alpha}). \tag{8}$$

Using this angle, the flux sector number (1 to 6) is determined by using the flux sector algorithm [17]. Therefore, two digits produced by hysteresis controllers and one by flux position are collectively used to trigger the switches of the VSI which selects the appropriate voltage vector by using the classical DTC lookup table [19]. Fig. 2 shows the possible voltage vectors which are employed in the DTC scheme. The appropriate voltage vector in each sampling period is selected in such a way that the torque and flux remain within their respective band limits.

C. Torque Ripple Analysis

Under the influence of any active VSI voltage vector, the motor torque keeps on increasing or decreasing until it touches the boundary defined by torque hysteresis bands. The torque ripple is only affected by the width of the torque hysteresis band and is almost independent of the width of the flux hysteresis band [21]. Torque ripple changes proportionally with change in the torque hysteresis bandwidth. However, due to the discrete nature of the control system, there might be still torque ripples even with the zero bandwidth of the hysteresis controller. On the other hand, if the bandwidth decreases, the VSI switching frequency increases, which proportionally increases its switching losses. Consequently, the bandwidth of the torque hysteresis controller must be optimized in such as a way that the torque ripple level and switching frequency of the inverter are within acceptable limits. A too small band may result in the selection of reverse voltage vector instead of zero vector to reduce the torque. The selection of reverse voltage vector may then cause torque undershoot. Hence, the torque ripple will become higher than those specified by the hysteresis controller band limits. The

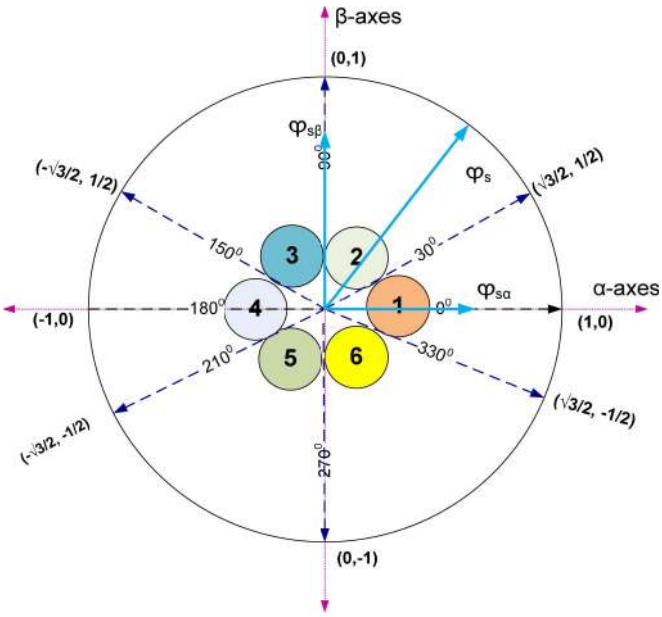

Fig. 3. Stator flux-linkage vector with six sectors. The stator flux-linkage vector with its coordinates is shown at the boundary of each sector.

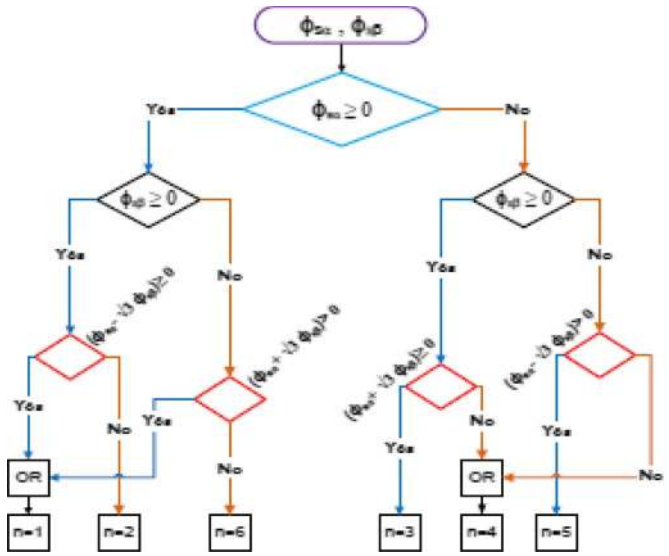

Fig. 4. Flow diagram for flux sector number determination.

torque slope is a function of motor speed, stator voltage and flux, and rotor flux vector and is given by [22]

$$\text{slope}^{+} = -\frac{T_e(n)}{\sigma\tau_{\text{sr}}} + \frac{3PL_m}{2\sigma L_s L_r}\left[(V_s - j\omega_m\phi_s).j\phi_r\right] \quad (9)$$

$$\text{slope}^{-} = -\frac{T_e(n)}{\sigma\tau_{\text{sr}}} + \frac{3PL_m}{2\sigma L_s L_r}\left[(-j\omega_m\phi_s).j\phi_r\right] \quad (10)$$

where $T_e(n)$ is the nth sample of torque and ω_m is the rotor speed. Both of these equations are speed dependent, but at lower speed range, the positive slope is greater than the negative slope. It means that the time taken by torque to reach upper and lower band limits, as well as switching frequency, varies with the rotor speed.

III. Proposed Flux-Linkage Sector Algorithm

The stator flux-linkage space vector with its coordinates in complex plane at the boundary of each sector is shown in Fig. 3. For simplicity, the amplitude of the stator flux-linkage vector is considered unity. Using these coordinates and the flow diagram of Fig. 4, the present sector number "n" of the stator flux vector can easily be determined. This algorithm uses only simple comparator operators and no trigonometric relation, as used by the conventional flux sector algorithm (8). For example, if both $\phi_{s\alpha}, \phi_{s\beta}$ are greater than zero and the term $(\phi_{s\alpha} - \sqrt{3}\,\phi_{s\beta})$ is also greater than zero, then the current sector number "n" will be "1."

IV. Design of FLC for Torque Ripple Optimization

In this paper, a Mamdani-type FLC is developed to adapt the torque hysteresis band in order to reduce the ripples in the motor-developed torque [23]–[25]. In conventional DTC technique, the amplitude of the torque hysteresis band is fixed. However, in this proposed scheme, the FLC controls the upper and lower limits of the torque hysteresis band on the basis of its feedback inputs. The fuzzy systems are universal function approximators [24]. The FLC is used as a nonlinear function approximator producing a suitable change in the bandwidth of the torque hysteresis controller in order to keep the torque ripples minimum. There are five membership functions for one input (dT_e) and three membership functions for another input (dI_s). Automatically, there will be fifteen rules. For the inputs, we use triangular/trapezoidal membership functions in order to reduce the computational burden. However, Gaussian membership functions are chosen for the output so that the hysteresis bandwidth will be changed smoothly. The nonlinear mapping from the input to the output of FLC is done by trial and error and experience basis. First, the membership functions and fuzzy rules were developed in simulation program by trial-and-error method so that the motor can follow the command speed with optimum level of torque ripples. Then, these fuzzy rules are applied in real-time program. From Faraday's electromagnetic theory for coil wound on unsaturated magnetic material (linear range of magnetizing curve), the stator flux linkage is proportional to the stator current. Therefore, the motor-estimated torque (6) variation (dT_e) and stator current variation (dI_s) over a sampling period are chosen as inputs to the FLC which can be defined by the following equations:

$$dT_e = T_e[n] - T_e[n-1] \quad (11)$$

$$dI_s = I_s[n] - I_s[n-1] \quad (12)$$

where $T_e[n]$ and $T_e[n-1]$ present the present and previous samples of motor-estimated torque, respectively. The motor mechanical equation, neglecting the friction coefficient, can be written as [17]

$$T_e - T_L = J\frac{d\omega_r}{dt}. \quad (13)$$

Combining (9), (10), and (13) leads to the conclusion that reducing the motor torque ripples directly reduces the motor

Fig. 5. Block diagram of the proposed FLC for hysteresis band adaptation.

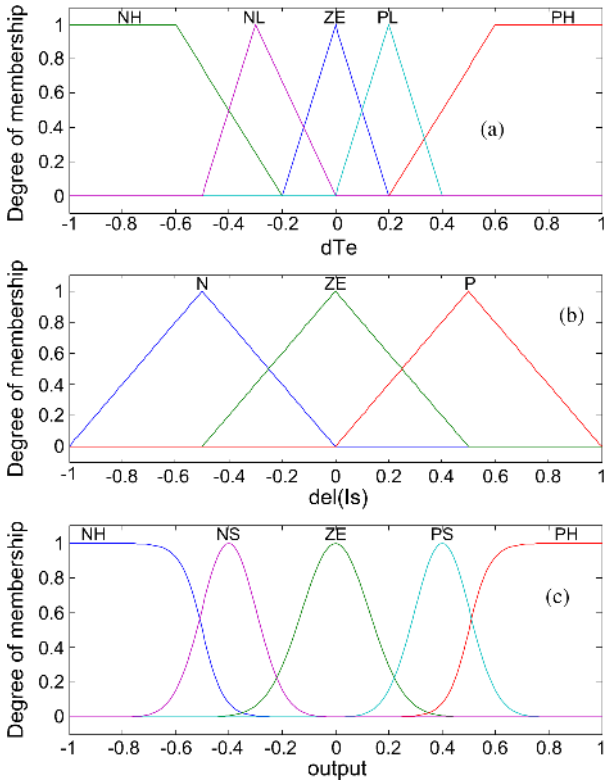

Fig. 6. Membership functions for input/output variables of FLC. (a) dT_e. (b) dI_s. (c) ΔHB_T.

speed ripples as well. The output of the FLC is the change in torque hysteresis bandwidth "ΔHB_T." The updated upper and lower bandwidths of the torque hysteresis controller are obtained as

$$HB^n_{\mathrm{TU}} = HB_{\mathrm{TU}} - K^*_U \Delta HB_T \tag{14}$$

$$HB^n_{\mathrm{TL}} = HB_{\mathrm{TL}} + K^*_L \Delta HB_T \tag{15}$$

where HB_{TU} and HB_{TU} are the base fixed upper and lower bandwidths of the torque hysteresis comparator. K_U and K_L are the scaling factors. The FLC is designed on the basis of observation of simulation results of the conventional DTC-based drive. The amount of positive torque ripple varies inversely with the load and speed. The reverse is the case for the negative torque slope. The block diagram of FLC is shown in Fig. 5 while the membership functions of the input and output variables of FLC are shown in Fig. 6. The fuzzy rules employed are as follows.

1) If dT_e is ZE and dI_s is N, then ΔHB_T is ZE.
2) If dT_e is ZE and dI_s is ZE, then ΔHB_T is ZE.
3) If dT_e is ZE and dI_s is P, then ΔHB_T is ZE.
4) If dT_e is PL and dI_s is N, then ΔHB_T is PS.
5) If dT_e is PL and dI_s is ZE, then ΔHB_T is PH.
6) If dT_e is PL and dI_s is P, then ΔHB_T is PH.
7) If dT_e is PH and dI_s is N, then ΔHB_T is PH.
8) If dT_e is PH and dI_s is ZE, then ΔHB_T is PH.
9) If dT_e is PH and dI_s is P, then ΔHB_T is PH.
10) If dT_e is NL and dI_s is N, then ΔHB_T is NH.
11) If dT_e is NL and dI_s is ZE, then ΔHB_T is NH.
12) If dT_e is NL and dI_s is P, then ΔHB_T is NS.
13) If dT_e is NH and dI_s is N, then ΔHB_T is NH.
14) If dT_e is NH and dI_s is ZE, then ΔHB_T is NH.
15) If dT_e is NH and dI_s is P, then ΔHB_T is NH.

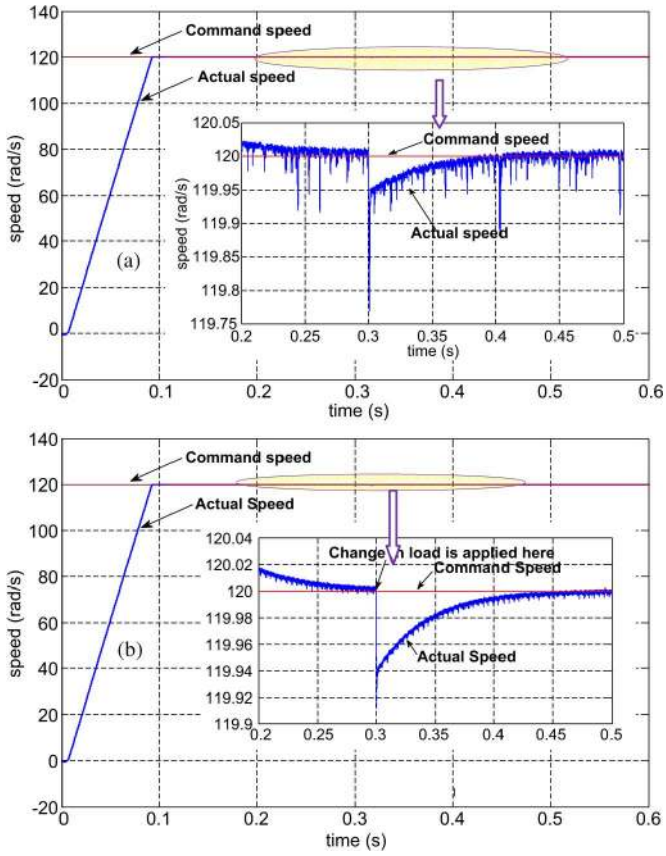

Fig. 7. Speed responses of the IM drive with zoom-in view for the highlighted portion, for change in load from 0.3 to 0.8 N · m at speed of 120 rad/s. (a) Conventional DTC. (b) FLC-based DTC.

V. Simulation Results

The performance of the proposed FLC-based DTC scheme for IM drive has been investigated extensively at different operating conditions. Sample simulations results are presented below. The nominal IM parameters, used for simulation and real-time application, are given in the Appendix.

Figs. 7–9 show the various IM drive responses for step change in motor load from 0.3 to 0.8 N · m. The change in load is applied at a time of 0.3 s. Fig. 7 shows the simulated speed response, with zoom-in view for interval of 0.2 to 0.5 s, using the conventional and the proposed DTC schemes. The zoom-in view of each speed response clearly shows that both the speed undershoot and speed ripples have been reduced considerably by the use of the proposed scheme. The undershoot and average speed ripples with the conventional DTC scheme are approximately 0.23 and 0.05 rad/s, respectively. The use of the proposed scheme has reduced these values to 0.09 and

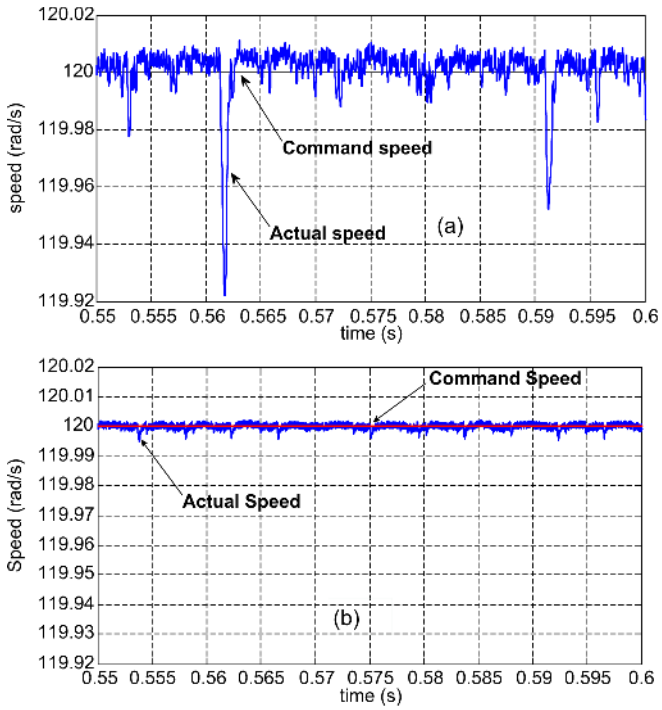

Fig. 8. Steady-state speed responses of the IM drive for a step change in load from 0.3 to 0.8 N · m at 120 rad/s. (a) Conventional DTC. (b) FLC-based DTC.

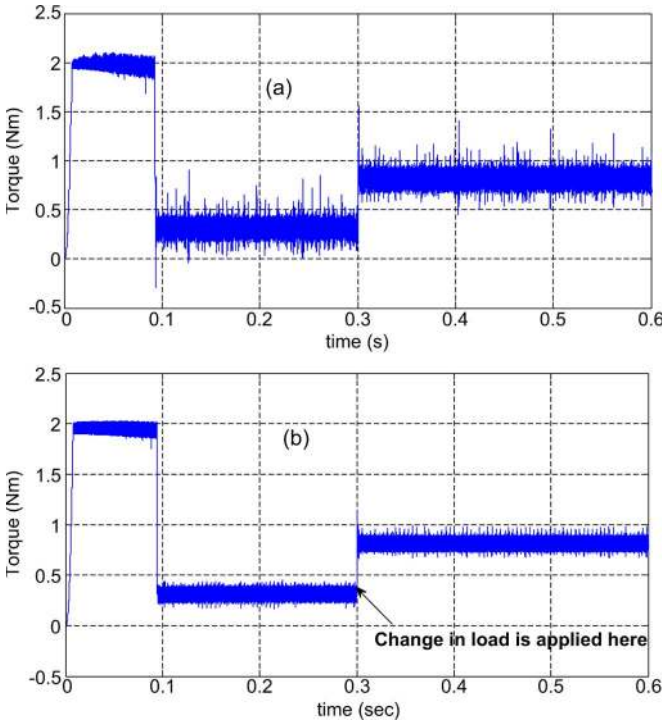

Fig. 9. Developed torque responses of the IM drive for a step change in load from 0.3 to 0.8 N · m at speed of 120 rad/s. (a) Conventional DTC. (b) FLC-based DTC scheme.

0.005 rad/s, respectively. Fig. 8 shows the steady-state speed responses. The conventional DTC scheme has approximate average speed ripples of 0.02 rad/s with some very big abrupt peaks. By using the proposed DTC scheme, the speed response is very smooth, and there are almost negligible ripples. Fig. 9 shows the corresponding torque responses for the conventional

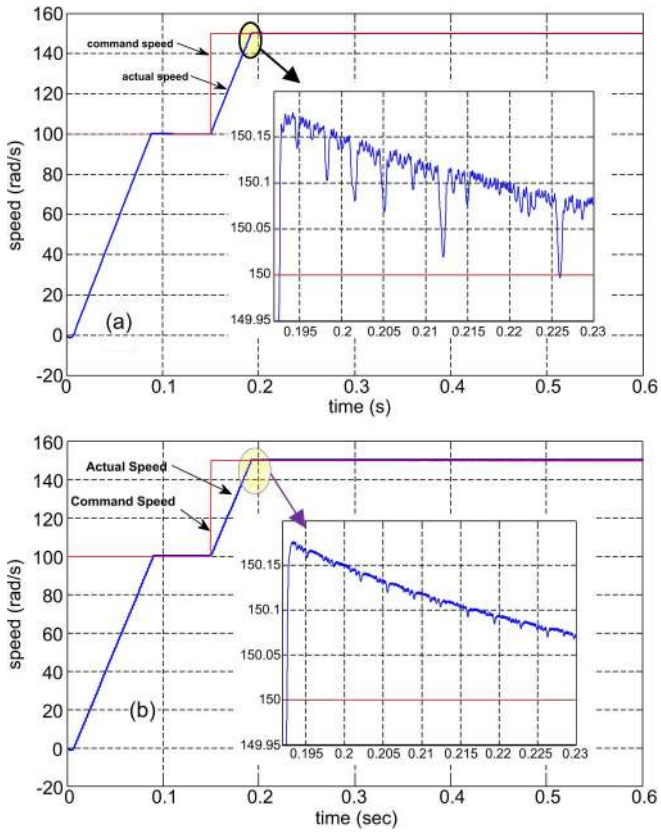

Fig. 10. Speed responses of the IM drive with zoom-in view of the encircled portion of the response, for a step change in command speed from 100 to 150 rad/s at a 0.5-N · m load. (a) Conventional DTC. (b) FLC-based DTC scheme.

and the proposed DTC schemes for a step change in load at 0.3 s. The torque ripple has significantly been reduced in the proposed scheme both in the transient and steady states. In particular, the negative torque ripple is very big in the conventional DTC scheme.

Figs. 10 and 11 show the simulation responses for a step change in command speed from 100 to 150 rad/s at $t = 0.15$ s while the motor is running at a 40% rated load (0.5 N · m). Fig. 10 shows the speed responses for the conventional and the proposed DTC-based IM drive. The proposed scheme shows better response as compared to the conventional one in terms of speed ripple during transient condition. Fig. 11 presents the corresponding torque response of the two DTC schemes. It can be compared that, in the steady state, the torque ripple in the conventional scheme is approximately 0.5 N · m while, in the proposed scheme, it is only 0.2 N · m, which proves the superiority of the proposed DTC scheme over the conventional one.

Figs. 12 and 13 show the flux and current responses of the drives for a 40% load while the motor is running at 120 rad/s. Fig. 12 shows the stator flux responses of both the conventional and proposed DTC schemes. It is found that the proposed variable band torque hysteresis controller-based DTC scheme exhibits smooth response and lesser ripple in flux as compared to the conventional DTC scheme. Fig. 13 shows the phase-a stator current of the conventional and proposed IM drives. The proposed scheme has lesser ripples in steady-state current.

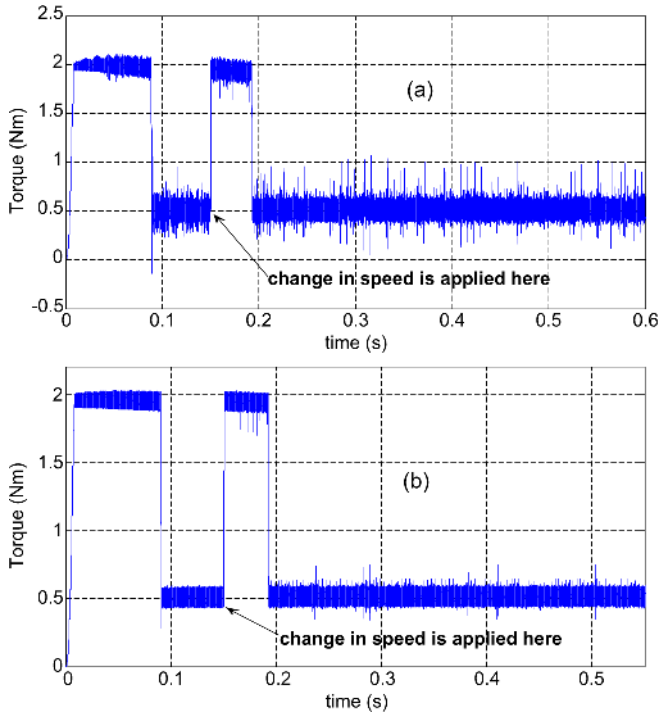

Fig. 11. Developed torque of the IM drive at 40% of rated load. The step change in speed from 100 to 150 rad/s is applied at 0.15 s. (a) Conventional DTC. (b) FLC-based DTC scheme.

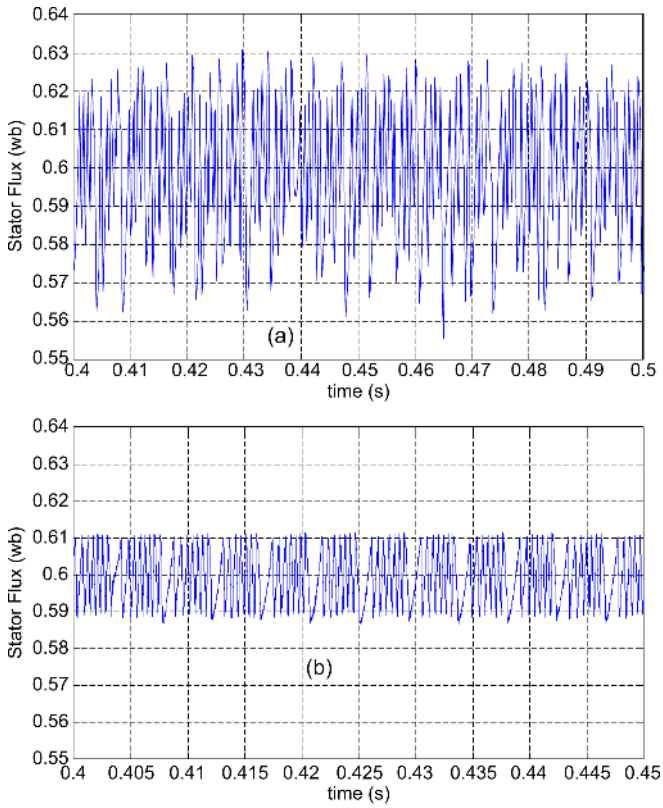

Fig. 12. Steady-state stator flux-linkage responses of the IM drive, at 40% rated load and speed of 120 rad/s. (a) Conventional DTC. (b) Proposed FLC-based DTC scheme.

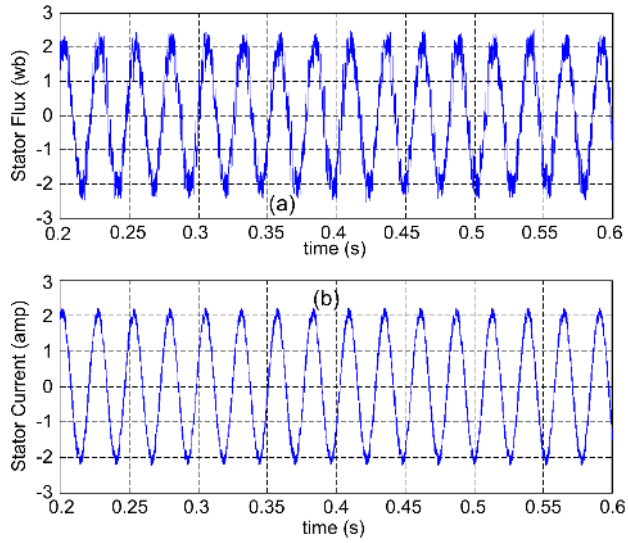

Fig. 13. Steady-state stator current response of the IM drive at 40% rated load and speed of 120 rad/s. (a) Conventional DTC. (b) FLC-based DTC scheme.

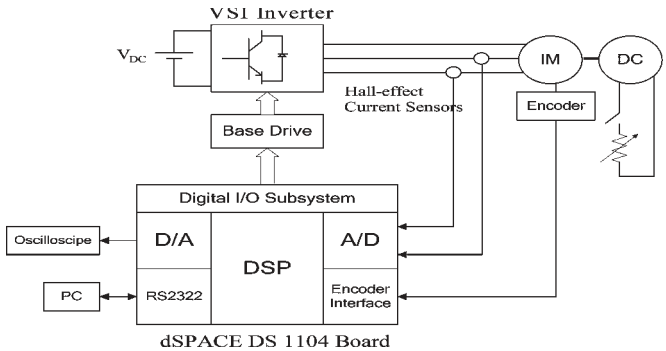

Fig. 14. Hardware schematic diagram for experimental setup.

Fig. 15. Snapshot of the experimental setup.

VI. Experimental Results

The proposed FLC-based DTC scheme for IM drive is experimentally implemented using DSP controller board DS-1104 for a laboratory 1/3 hp IM. Figs. 14 and 15 show the hardware schematic and snapshot of the experimental setup for the proposed FLC-based DTC scheme, respectively. The

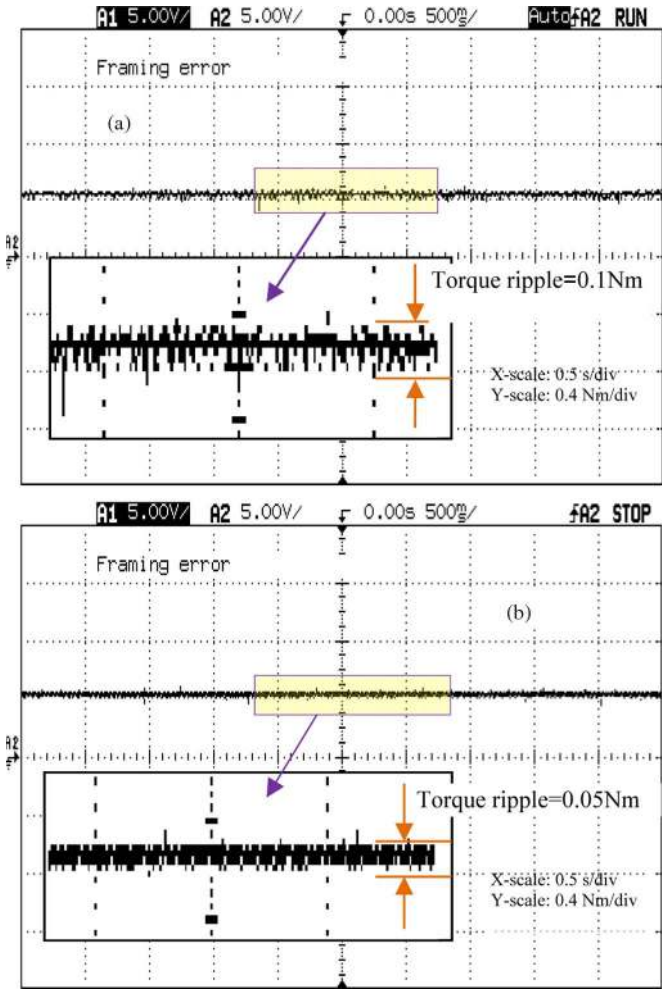

Fig. 16. Steady-state experimental torque responses of the IM drive with zoom-in view of the shaded portion, for command rated speed of 180 rad/s at 0.4-N · m load. (a) Conventional DTC. (b) FLC-based DTC.

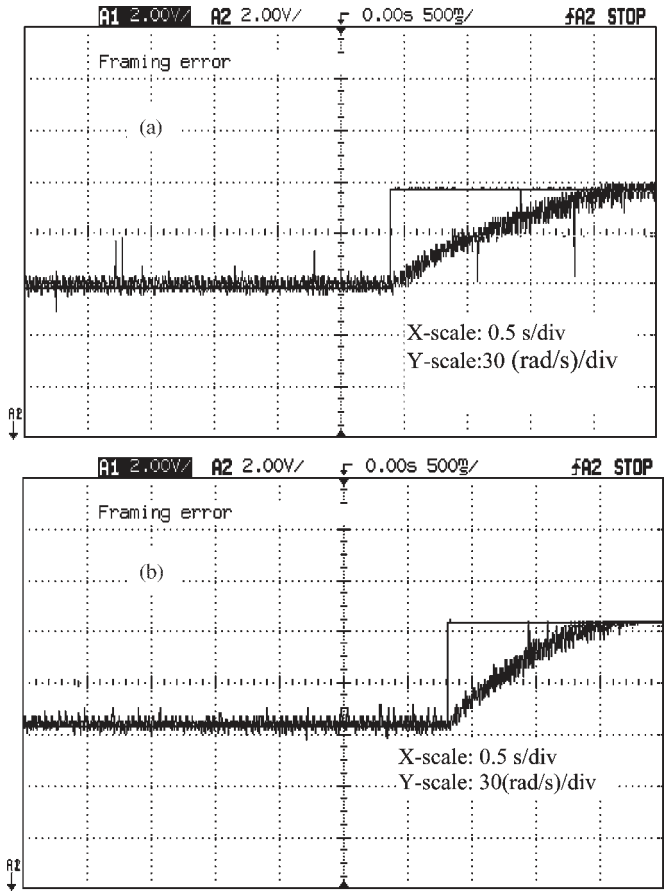

Fig. 17. Speed response for a step change in speed from 120 to 180 rad/s at 0.4-N · m load. (a) Conventional DTC. (b) FLC-based DTC.

sampling frequency obtained for this work is 10 kHz. Sample experimental results are presented hereinafter.

Fig. 16(a) and (b) show the real-time torque responses in steady state while the motor is following a command speed of 180 rad/s at a 0.4-N · m load, for the conventional and FLC-based DTC schemes, respectively. It is clearly seen that the proposed FLC-based DTC scheme has lesser torque ripple in the steady state. Fig. 17(a) and (b) shows the transient speed responses for a step change in speed from 120 to 180 rad/s at a 0.4-N · m load with the conventional and proposed DTC schemes, respectively. The use of proper voltage vector by the band-adapted FLC-based DTC scheme has reduced both the rise and the settling time. Moreover, the ripple level has also been reduced in the response with the proposed scheme. Thus, the effectiveness of the proposed FLC-based band-adapted hysteresis controller for DTC-based IM drive is verified by experimental results.

VII. Conclusion

A novel FLC-based DTC scheme for IM drive has been presented in this paper. The proposed FLC-based IM drive has been successfully implemented in real time using DSP board DS1104 for a laboratory 1/3 hp IM. The FLC is used to adapt the bandwidth of the torque hysteresis controller in order to reduce the torque ripple of the motor. A performance comparison of the proposed FLC-based DTC scheme with a conventional DTC scheme has also been provided both in simulation and experiment. Comparative results show that the torque ripple of the proposed drive has considerably been reduced. The dynamic speed response of the proposed FLC-based DTC scheme has also been found better as compared to the conventional DTC scheme.

Appendix

IM parameters used for experiment: Lls $= 0.0154$ H, Llr $= 0.0154$ H, $L_m = 0.2655$ H, $P = 2$, $R_s = 6.5\ \Omega$, $R_r = 3.4\ \Omega$, $J = 0.0012$ kg · m^2, $B_m = 0.0001$ N · m/rad/s, and HP $= 1/3$.

Torque hysteresis controller parameters: $HB_{\mathrm{TU}} = 0.1$, $HB_{\mathrm{TL}} = -0.1$, $K_U = 1$, and $K_L = 2$.

References

[1] I. Takahashi and T. Nouguchi, "A new quick response and high efficiency control strategy for an induction motor," *IEEE Trans. Ind. Appl.*, vol. IA-22, no. 5, pp. 820–827, Sep. 1986.

[2] L. Tang, L. Zhong, M. F. Rahman, and Y. Hu, "A novel direct torque control for interior permanent-magnet synchronous machine drive with low ripple in torque and flux-a speed-sensorless approach," *IEEE Trans. Ind. Appl.*, vol. 39, no. 6, pp. 1748–1756, Sep./Oct. 2003.

[3] S. Kouro, R. Bernal, H. Miranda, C. A. Silva, and J. Rodriguez, "High-performance torque and flux control for multilevel inverter fed induction motors," *IEEE Trans. Power Electron.*, vol. 22, no. 6, pp. 2116–2123, Nov. 2007.
[4] D. Casadei and T. Angelo, "Implementation of a direct torque control algorithm for induction motors based on discrete space vector modulation," *IEEE Trans. Power Electron.*, vol. 15, no. 4, pp. 769–777, July 2000.
[5] C.-T. Lin and C. S. G. Lee, *Neural Fuzzy Systems: A Neuro-Fuzzy Synergism to Intelligent Systems*. Upper Saddle River, NJ: Prentice-Hall, 1996.
[6] Y.-S. Lai and J.-C. Lin, "New hybrid fuzzy controller for direct torque control induction motor drives," *IEEE Trans. Power Electron.*, vol. 18, no. 5, pp. 1211–1219, Sep. 2003.
[7] L. Youb and A. Craciunescu, "Direct torque control of induction motors with fuzzy minimization torque ripple," in *Proc. WESCO*, 2009, vol. 2, pp. 713–717.
[8] A. F. Aimer, A. Bendiabdellah, A. Miloudi, and C. Mokhtar, "Application of fuzzy logic for a ripple reduction strategy in DTC scheme of a PWM inverter fed induction motor drives," *J. Elect. Syst.*, Special Issue 1, pp. 13–17, Nov. 2009.
[9] G. Sheng-wei and C. Yan, "Research on torque ripple minimization strategy for direct torque control of induction motors," in *Proc. ICCASM*, 2010, pp. VI-278–VI-281.
[10] G. M. Gadoue, D. Giaouris, and J. W. Finch, "Artificial intelligence-based speed control of DTC induction motor drives—A comparative study," *Elect. Power Syst. Res.*, vol. 79, no. 1, pp. 210–219, 2009.
[11] R. Toufouti, S. Meziane, and H. Benalla, "Direct torque control for induction motor using fuzzy logic," *ACSE J.*, vol. 6, no. 2, pp. 19–26, Jun. 2006.
[12] F. Sheidaei, M. Sedighizadeh, S. H. Mohseni-Zonoozi, and Y. Alinejad-Beromi, "A fuzzy logic direct torque control for induction motor sensorless drive," in *Proc. UPEC*, 2007, pp. 197–202.
[13] Y. V. S. Reddy, M. Vijayakumar, and T. Brahmananda Reddy, "Direct torque control of induction motor using sophisticated lookup tables based on neural networks," *AIML J.*, vol. 7, no. 1, pp. 9–15, Jun 2007.
[14] J.-K. Kang, D.-W. Chung, and S.-K. Sul, "Direct torque control of induction machine with variable amplitude control of flux and torque hysteresis bands," in *Proc. IEMD*, 1999, pp. 640–642.
[15] K.-K. La, M.-H. Shin, and D.-S. Hyun, "Direct torque control of induction motor with reduction of torque ripple," in *Proc. IEEE IECON*, 2000, pp. 1087–1092.
[16] J.-K. Kang and S.-K. Sul, "New direct torque control of induction motor for minimum torque ripple and constant switching frequency," *IEEE Trans. Ind. Appl.*, vol. 35, no. 5, pp. 1076–1082, Sep./Oct. 1999.
[17] P. Vas, *Sensorless Vector and Direct Torque Control*. London, U.K.: Oxford Univ. Press, 1998.
[18] A. E. Fowkes, "Hardware efficient algorithm for trigonometric functions," *IEEE Trans. Comput.*, vol. 42, no. 2, pp. 235–239, Feb. 1993.
[19] H. F. Abdul Wahab and H. Sanusi, "Simulink model of direct torque control of induction machine," *Amer. J. Appl. Sci.*, vol. 5, no. 8, pp. 1083–1090, 2008.
[20] A. M. Trzynadlowshi, *The Field Orientation Principle in Control of Induction Motors*. Norwell, MA: Kluwer, 1994.
[21] D. Casadei, G. Grandi, G. Serra, and A. Tani, "Effects of flux and torque hysteresis band amplitude in direct torque control of induction machines," in *Proc. IEEE IECON*, 1994, vol. 1, pp. 299–304.
[22] N. Rumzi, N. Idris, and A. H. M. Yatim, "Direct torque control of induction motors with constant switching frequency and reduced torque ripple," *IEEE Trans. Ind. Electron.*, vol. 51, no. 4, pp. 758–767, Aug. 2004.
[23] P. Vas, *Artificial-Intelligence-Based Electrical Machines and Drives*. New York: Oxford Univ. Press, 1999.
[24] C. C. Lee, "Fuzzy logic in control systems: Fuzzy logic controller—Part I," *IEEE Trans. Syst., Man, Cybern.*, vol. 20, no. 2, pp. 404–418, Mar./Apr. 1990.
[25] K. M. Passino and S. Yurkovich, *Fuzzy Control*. Menlo Park, CA: Addison-Wesley Longman, 1998, p. 72.

M. Nasir Uddin (S'98–M'00–SM'04) received the B.Sc. and M.Sc. degrees in electrical and electronic engineering from Bangladesh University of Engineering and Technology (BUET), Dhaka, Bangladesh, in 1993 and 1996, respectively, and the Ph.D. degree in electrical engineering from Memorial University of Newfoundland (MUN), St. John's, NL, Canada, in 2000.

He is currently a Professor in the Department of Electrical Engineering, Lakehead University (LU), Thunder Bay, ON, Canada. He was a Visiting Professor (June–December 2011) at the University of Malaya, Kuala Lumpur, Malaysia, during his sabbatical leave from Lakehead. Previously, he served as an International Visiting Professor (June–July 2010) at Tokyo University of Science, Suwa, Japan, and a Visiting Associate Professor (July–December 2006) at North South University, Dhaka. Previously, he was an Assistant Professor in the Department of Electrical and Computer Engineering, University of South Alabama, Mobile, from January 2001 to May 2001, a Postdoctoral Fellow at MUN from May 2001 to August 2001, and an Assistant Professor from 1996 to 1997 and a Lecturer from 1994 to 1996 at BUET. He also served as an Instructor from 1999 to 2000 at the College of the North Atlantic, St. John's, Canada. He possesses more than 15 years of teaching experience and has authored or coauthored over 120 papers in international journals and conference proceedings. His research interests include power electronics, electric motor drives, and the application of intelligent controllers.

Dr. Uddin is a Registered Professional Engineer in the Province of Ontario, Canada. Currently, he is serving as Chair of the IEEE Industry Applications Society (IAS) Industrial Automation and Control Committee (IACC). He is the Technical Chair for the IEEE IAS (IACC) Annual Meetings 2011 and 2012. Previously, he was the TRANSACTIONS Review Chair for IEEE/IAS/IACC. Recently, he was bestowed upon with the prestigious Lakehead University Distinguished Researcher Award 2010. He is the recipient of two First Prize and one Third Prize Paper Awards from the IEEE/IAS/IACC and both 2004 Contributions to Research Award and Contributions to Teaching Award from LU.

Muhammad Hafeez received the B.Sc. degree in electrical engineering from the University of Engineering and Technology, Lahore, Pakistan, in 1992, and the M.Sc. degree in control engineering from Lakehead University, Thunder Bay, ON, Canada, in 2010.

He served as an Electrical Engineer for the Water and Power Development Authority, Pakistan (May 1992–February 2002). He possesses more than nine years of experience in maintenance, troubleshooting, and commissioning of electrical power generating stations. He is currently with the Thunder Bay Regional Research Centre, Thunder Bay. His research interests include electric motor drives and the application of intelligent controllers.